Converging Flows of Viscoelastic Materials

A. B. METZNER, E. A. UEBLER, and C. F. CHAN MAN FONG
University of Delaware, Newark, Delaware

The kinematics of converging velocity fields such as those found in flows from a large duct or reservoir into a small tube are especially simple in the case of viscoelastic materials as they may be approximated by means of a diagonal deformation rate tensor. This result is shown to be valid in the present study in which aqueous polymeric solutions were utilized and is inferred as having been valid under the experimental conditions employed by Bagley in studies of molten polymers. It is suggested that asymptotic approximations based upon the diagonality of the deformation rate tensor may be of general use in analysis of flows of viscoelastic materials, that is, they could represent, potentially, simplifying approximations comparable in utility to the boundary layer approximations employed commonly in the analysis of flows of Newtonian fluids.

An interesting prediction of the present analysis is that for flows from a large duct into a small one a plot of isotropic pressure vs. axial position exhibits a minimum near the inlet to the smaller duct. Experimental results are presented in partial support of this unusual behavior. The analysis also suggests that an orifice jet thrust technique for measurement of normal stresses, closely related to recent independent studies by Middleman and by Fabula, may be an indirect but especially simple and sensitive tool for measurement of material properties.

The convergent velocity field formed when a Newtonian fluid flows from a larger duct or reservoir into a small tube is shown in Figure 1, the fluid motion being made visible by small illuminated particles which trace out the streamlines. It is seen that under the conditions used, typical of flows at very low Reynolds numbers, the fluid converges into the small duct through a full 180 deg. solid angle. At larger Reynolds numbers small vortices may form in the corners of the upstream chamber, depending upon its size and geometry, but the basic features of the flow remain unaltered: in all cases the fluid in the entire region immediately upstream from the small duct moves toward the entry. If the small duct protrudes upstream into the larger chamber, rather than being coplanar with the entry as in Figure 1, the fluid converges into the small duct through a full 360 deg. solid angle, as shown in Figure 3, but otherwise the general features of the flow remain. In both cases the entire fluid region surrounding the opening to the small tube is in a state of motion with the local velocity vector directed toward the tube entry (*34*).

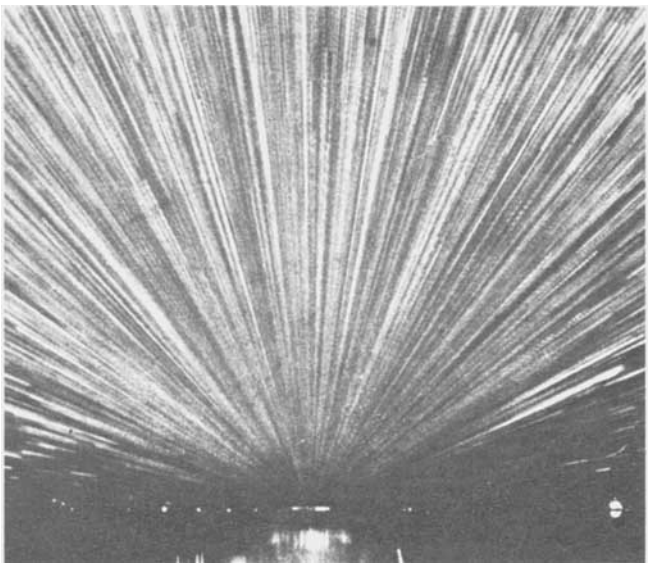

Fig. 1. Velocity field of Newtonian fluid (glycerin) upstream of an abrupt contraction at very low Reynolds numbers. Entry plane of small duct coplanar with downstream face of large reservoir. Data of H. Giesekus.

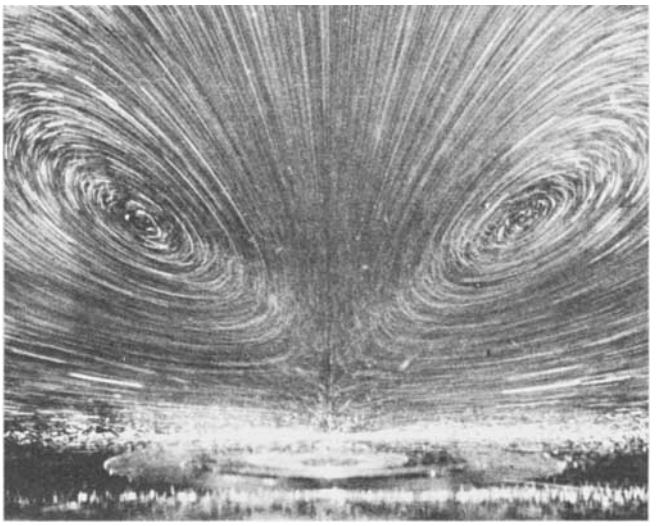

Fig. 2. Velocity field of viscoelastic fluid (1.67% aqueous solution of polyacrylamide); flowrates similar to those of Figure 1. Data of H. Giesekus.

In contrast to the above Figure 2 depicts the behavior of a viscoelastic polymeric solution under kinematic conditions similar to those used for the Newtonian fluid of Figure 1. The differences are dramatic. In this instance the fluid entering the small tube is restricted to that initially present upstream in a very slender conical region. The regions of secondary flow, not visible at all in Figure 1 and small in extent when present at higher Reynolds numbers in Newtonian fluids, are of primary importance in the viscoelastic case as they occupy a major part of the upstream duct or reservoir.

These general differences between Newtonian and viscoelastic fluids in converging flows have been the subject of much qualitative study; engineers and scientists interested in extrusion and melt fracture problems in the processing of polymers have long been aware of them (*4, 8,* 33). Analytically, however, progress has been tedious and difficult; while the qualitative features noted above have been predicted for flow in a converging two-dimensional channel (*17*) as well as in a conical geometry (*18,* 32) the approximations used to describe the fluid properties are valid only for very slow flows. In Kaloni's work (*17, 18*) an asymptotic expansion valid for small Deborah numbers (23) was used while in Schümmer's study the constitutive properties were assumed to be those of a third-order fluid, an approximation also useful in description of real materials only in the limit of very low deformation rates (*23*). A recent study of Fields and Bogue

E. A. Uebler is with E. I. duPont de Nemours and Company, Wilmington, Delaware and C. F. Chan Man Fong is with The University of Reading, Reading, England.

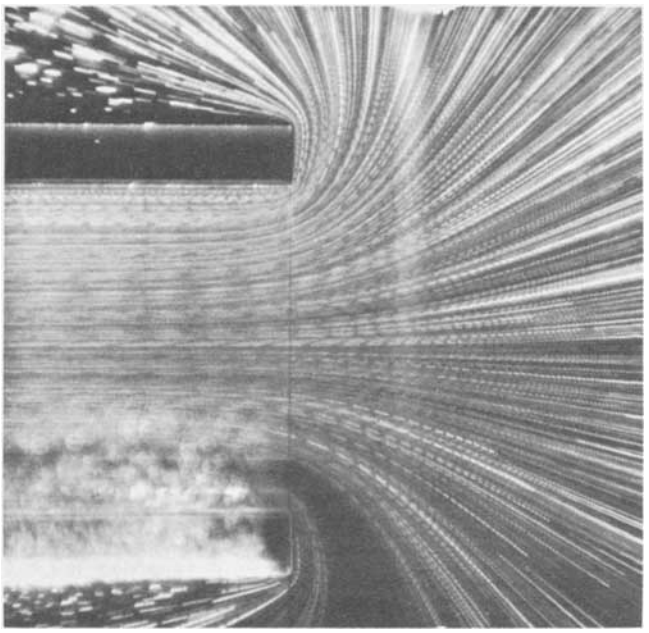

Fig. 3. Velocity field of Newtonian fluid in vicinity of abrupt contraction. Small duct protrudes into upstream reservoir. $N_{Re} = 0(10^2)$.

(*14*) includes terms of higher order and though it considers only the stress field along the centerline of the system it will be seen that this is not a serious restriction. The purpose of the present work is to extend these prior studies, both analytically and experimentally, to what is perhaps the more interesting asymptotic extreme of very rapid flows.

EXPERIMENTAL STUDY OF KINEMATICS OF CONVERGING FLOWS

Figures 3 to 5 depict the details of the velocity field in the immediate vicinity of the entrance to the smaller duct. In these figures the upstream end of the smaller duct was made to project into the upstream reservoir,

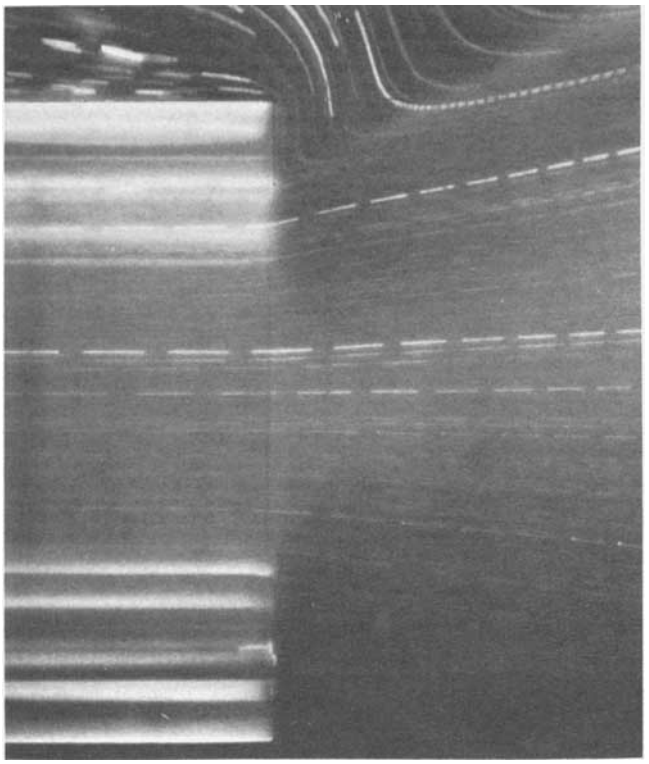

Fig. 4. Velocity field of viscoelastic fluid, $q = 7.25$ gal./min.

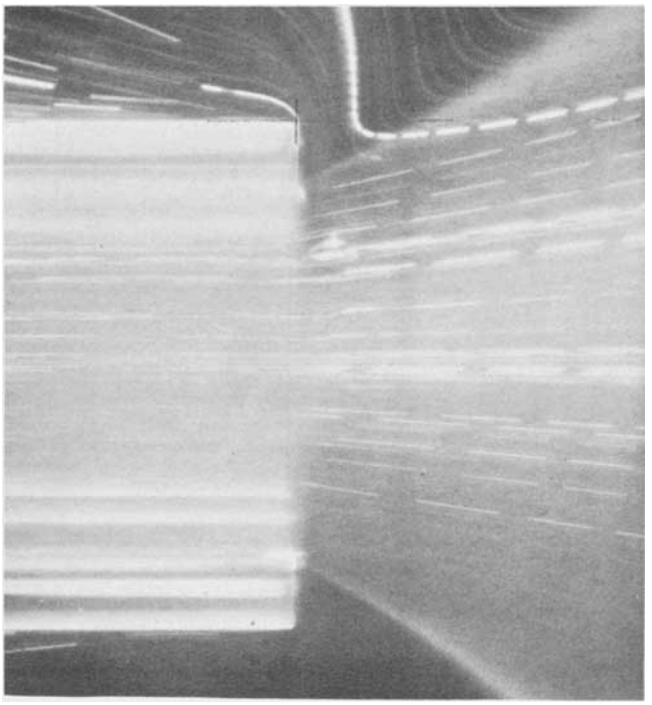

Fig. 5. Velocity field of viscoelastic fluid, $q = 21.75$ gal./min.

rather than being coplanar with the downstream end of the latter as in Figures 1 and 2, so that the detailed velocity field could be studied photographically very near the small tube entry without gaskets or walls obscuring the view. These figures show that the general differences between Newtonian and viscoelastic fluids noted above are retained in this geometry and that, in addition, an increasingly intense haze is developed in the converging viscoelastic fluid as the flowrate increases. The causes of this important observation will become clear later. The

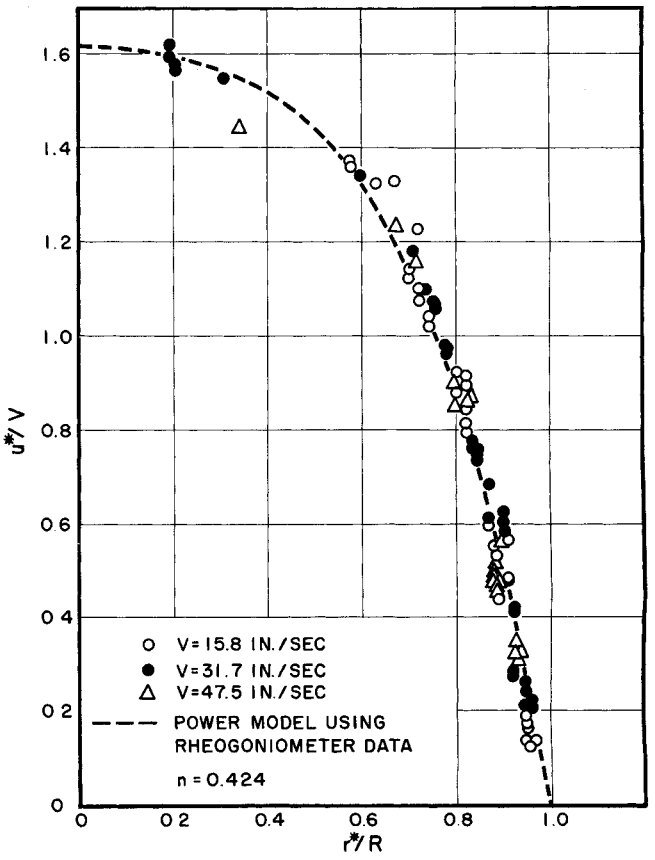

Fig. 6. Profile of well-developed axial velocities, viscoelastic fluids. Data taken 28 tube radii downstream from entry.

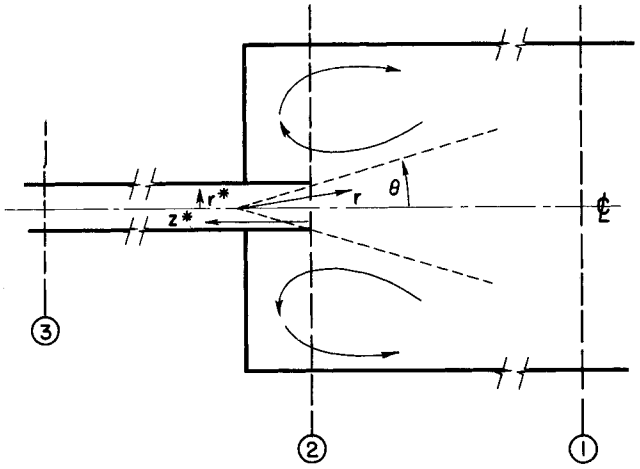

Fig. 7. Coordinate systems used in analysis.

experimental conditions under which these photographs were taken are detailed in Table 1.

TABLE 1. EXPERIMENTAL CONDITIONS CORRESPONDING TO FIGURES 3 TO 5

Newtonian fluid: 70% Globe brand white corn syrup in water: $\mu = 1.96$ poise
Viscoelastic fluid: 0.5% Separan AP 30, a partially hydrolyzed polyacrylamide, in water
Flow behavior index $n = 0.424$, measured rheogonimetrically*
Flow rates: Figure 3: 5.45 gal./min.
4: 7.25 gal./min.
5: 21.75 gal./min.
Geometry of equipment:
Downstream tube: I.D. = 1.48 in.
O.D. = 2.00 in.
Upstream reservoir: square cross section 18 in. on a side. A distributor plate, to develop equal axial velocities at all radial positions, was mounted 10 in. upstream from the entrance to the small tube.
Illumination: through the vertical central plane of the apparatus. Width (depth) of illuminated plane: 1/16 in.
Tracer particles: small air bubbles.
Temperature: all data reported were taken at 22.0 ± 2°C.

* Curves of both the shearing stress and the first normal stress difference are available for the non-Newtonian fluid used (*34*).

Measurements of the streak lengths on photographs such as these were made utilizing a 10-power travelling microscope. Over 100 photographs were taken, at several axial positions, for each flowrate, in order to obtain detailed point velocity measurements. Streak lengths were measured from leading edge to leading edge of the particles to eliminate errors due to finite particle size. The accuracy of the measurements may be judged in two ways. First, the velocities measured downstream may be compared with the well-developed velocity profile, calculating the latter from the viscosity function of the fluid as measured rheogoniometrically. The results of this comparison. given in Figure 6, are seen to be excellent. Secondly, the local velocities may be integrated over the cross section of the apparatus and the result compared with the known volumetric flow rate. This comparison, though less detailed, is of interest as it can be made in the upstream (Lagrangian accelerating) field as well as under the well-developed (Lagrangian steady) flow conditions within the downstream tube. The mean deviation of these integrated flow rates was less than 6% and all errors appeared to be random (*34*). It is concluded from these results that the velocity measurements to be reported are of a generally high accuracy, that is, that aberrations due to buoyancy or inertia did not occur.

The velocity field within the converging conical region of Figures 4 and 5 may be conveniently analyzed employing a spherical polar coordinate system with its origin located downstream within the small duct at a point determined by extending the converging streamlines in these figures to intersection, as shown in Figure 7. Distances upstream of this origin are denoted by r and will be normalized with respect to R, the radius of the small duct. Under the flow conditions studied the origin of this coordinate system, determined experimentally, was located along the centerline of the small duct approximately four tube radii downstream of the entry plane.

A tentative analysis of the observed velocity field suggested the flow upstream of the small duct to be radially directed toward the origin of this spherical coordinate system. If this is so the continuity equation gives:

$$ur^2 = f(\theta) \qquad (1)$$

and the conjecture may be tested by means of plots of local velocity vs. $1/r^2$. On logarithmic coordinates the slope of a plot of the dimensionless radial velocity u/V vs. r/R, the dimensionless radial position coordinate, will be equal to -2.00 if Equation (1) is obeyed. Figures 8 to 10 show the data of the present investigation; the curves drawn through the experimental points represent best fit straight lines as determined from a least squares analysis. The slopes of these lines were -1.96 at the lowest flow rate, -1.92 at the intermediate flow rate, and -1.85 at the highest flow rate, corresponding to generalized Reynolds numbers of 153, 490, and 845, respectively. It is clear that Equation (1) is at least approximately valid in the region $0 \leq \theta \leq 10$ deg. when θ is measured from the tube axis, and that $f(\theta)$ may be taken as a constant. This implies that the fluid is subject only to stretching or elongational modes of deformation, that is, that shearing deformations are negligibly small. At larger angular positions from the centerline, shearing deformations, though small, were large enough to be measured, but even under these conditions the assumption of radial flow was valid; it thus applies to substantially all the fluid which enters the downstream duct, under these experimental conditions of moderate to high flow

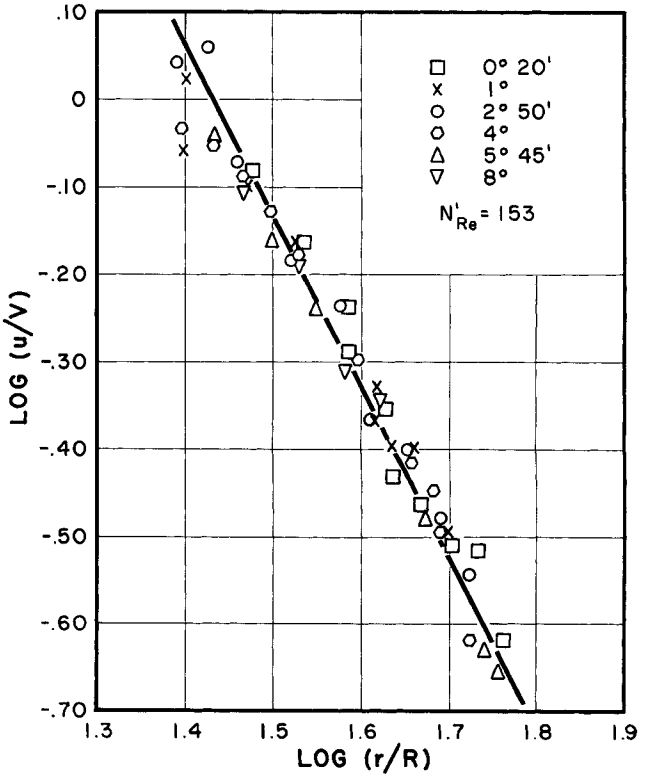

Fig. 8. Experimental test of Equation (1): $q = 7.25$ gal./min. (Coordinates for Figures 8-10 given in natural logarithms).

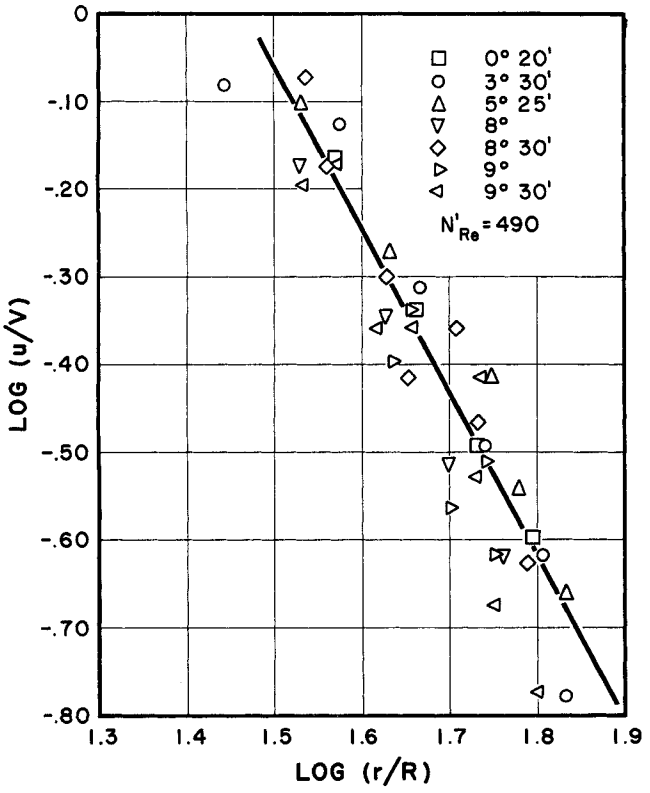

Fig. 9. Experimental test of Equation (1): $q = 14.50$ gal./min.

rates. The same is not true in the case of Newtonian fluids.

In the central conical region of the velocity field in which the fluid shearing deformations are negligibly small we may write Equation (1) as

$$u = \frac{Q}{r^2} \qquad (1a)$$

where $f(\theta)$ has been replaced by the constant Q which is proportional to the volumetric flow rate q. Under the conditions studied Equation (1a) applies to about 70% of all the fluid entering the tube from upstream. For purposes of further analysis we will restrict our attention to this central region ($0 \leq \theta \leq 10$ deg.); in this region the kinematics of the flow process, in spherical coordinates, are especially simple:

$$u_r = u = \frac{Q}{r^2} \qquad (1a)$$

$$u_\theta = u_\phi = 0 \qquad (1b)$$

These equations may be shown to give rise to a diagonal deformation rate tensor.

ANALYSIS OF STRESS AND PRESSURE FIELDS IN CONVERGING FLOWS

Overall Momentum Balances

Having defined the kinematics of the velocity field associated with flow from a large duct into a small one let us turn to a consideration of the stress field. As point values of the stresses have not been measured and are, in fact, very difficult to obtain even at low flow rates, it will be convenient to combine a stress analysis based on the diagonality of the deformation rate tensor with an overall momentum balance in order to be able to check stress predictions more simply by relating them to pressure drop–flow rate data which are obtainable with comparative ease. For this purpose we will introduce a second coordinate system based upon the natural cylindrical geometry of the duct. Confusion will be avoided if one remembers that constitutive equations utilizing the kinematics of Equations (1a) and (1b) and employed to predict the stress field will be based upon the spherical coordinate system r, θ, ϕ, implied in Equations (1a) and (1b); macroscopic momentum and pressure drop predictions will be based upon a cylindrical metric r^*, θ^*, z^* with its origin on the axis of the tube at its upstream end. Figure 7 depicts control surfaces useful in the overall macroscopic description of the problem. Section 1 is taken sufficiently far upstream to be outside the converging region near the inlet to the small tube. Section 2 is just at the entry plane to the tube and section 3 is taken far enough downstream for the velocity and stress fields to have become well-developed. Momentum balances may be written between these control surfaces; the following assumptions are utilized:

1. At section 1 the velocities and all stresses arising out of fluid deformation are negligibly small (that is, this upstream region may be considered to be of infinite cross-sectional area).

2. The velocities in the recirculating regions are negligibly small. Thus fluid momentum effects are negligible here and the small pressure differences across this annular region are neglected in writing the momentum balance.

3. At section 3 the velocity and stress fields may be calculated by using very simple empirical constitutive equations, since in the cylindrical tube only the region near the wall contributes strongly to the overall result. In particular power law approximations are entirely sufficient and will be used.

4. The viscous drag on the walls of the ducts will be neglected in the upstream region in which the velocities are low. In the small duct the value for well-developed flow will be employed as an approximation at all axial positions.

Under these assumptions and with A_1, A_2, and A_A denoting the cross-sectional areas of the upstream duct, the downstream tube (of radius R) and the annular region between the upstream duct and the tube at control surface 2, a momentum balance between control surfaces 1 and 2 yields:

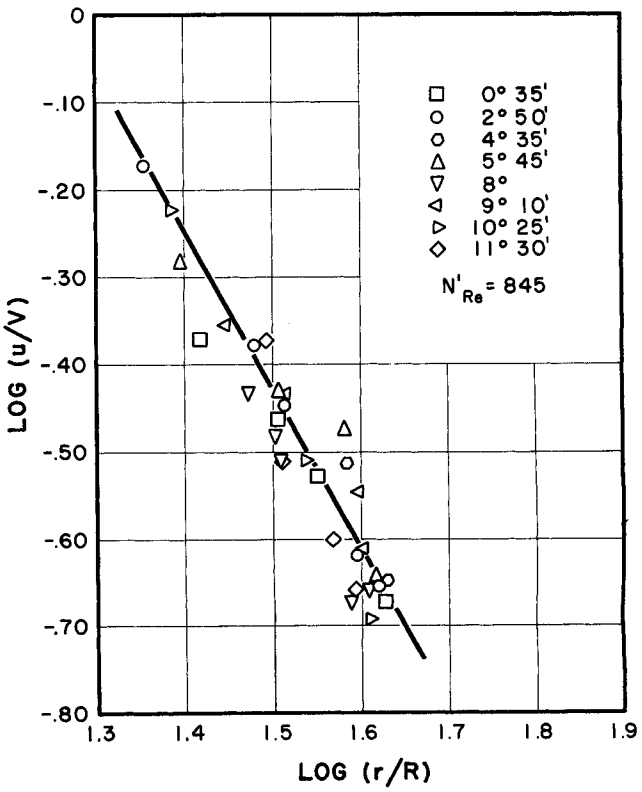

Fig. 10. Experimental test of Equation (1): $q = 21.75$ gal./min.

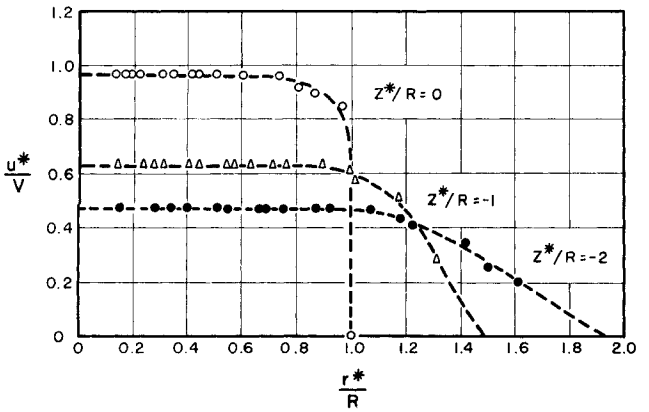

Fig. 11. Dimensionless axial velocity profiles through entrance region: q = 21.75 gal./min.

$$p_1 - p_{A2}\frac{A_A}{A_1} = \rho V^2 \frac{A_2}{A_1} - (\tau_{11})_2 \frac{A_2}{A_1} \qquad (2)$$

in which V denotes the mean velocity in the smaller tube and $(\tau_{11})_2$ is the total normal stress in the radial direction (in spherical coordinates) in the converging flow field at section 2. We emphasize again that radial flow here means fluid converging toward a point inside the tube. The usual rheological sign convention is used: positive normal stresses denote tensions in the fluid element. In this and what follows, the coordinate direction r will be denoted by 1, and the θ and ϕ directions by 2 and 3 respectively. The term p_{A2} denotes the stress which would be measured on a pressure tap at section 2, at any position external to the small tube. At section 2, the velocity inside the tube is essentially independent of position in the tube, that is, a flat velocity profile prevails. This is seen in Figure 11 in which the dimensionless axial velocity u^*/V is plotted vs. r^*/R. Thus in Equation (2) the local velocity is everywhere equal to V inside the tube at section 2 and the momentum flux term is just ρV^2. In writing Equation (2) the small differences between the radial stress and velocity, and their components in the z^* coordinate direction, have been neglected.

Considering the normal stress in the θ direction and dividing it into isotropic and deviatoric components we may write:

$$(\tau_{22})_2 = (-p)_2 + (P_{22})_2 \qquad (3)$$

Making the assumption that the flow in the annular region at section 2 is negligibly slow compared to that in the conical entry region, and therefore that the deviative normal stresses there are negligibly small, we may equate the θ directed normal stress within the conical region to the isotropic pressure outside the conical region in order to balance forces at the boundary. In particular,

$$(\tau_{22})_2 = -p_{A2} \qquad (3a)$$

Combining (3) and (3a),

$$-(p)_2 = -p_{A2} - (P_{22})_2 \qquad (4)$$

The normal stress $(\tau_{11})_2$ may therefore be written as

$$(\tau_{11})_2 = -(p)_2 + (P_{11})_2 \qquad (5)$$

$$= -p_{A2} + (P_{11} - P_{22})_2 \qquad (5a)$$

and the momentum balance [Equation (2)] can then be written

$$p_1 - p_{A2} = \rho V^2 A_2/A_1 - (P_{11} - P_{22})_2 A_2/A_1 \qquad (6)$$

When the inertial term is negligible, as in molten polymers, for example, Equation (6) indicates a pressure rise in the direction of flow: $p_{A2} > p_1$. This rise is small however, in view of the low value of the multiplier for the normal stress difference, $P_{11} - P_{22}$. Therefore, the initial neglect of this pressure difference in the momentum balance introduces only a higher-order error. However, it is not entirely of negligible importance physically as it provides the gradient for the upstream flow in the recirculating region near the walls of the large duct. The reason for this apparent pressure rise is that the converging stream of fluid is not so much being *pumped* forward into the smaller tube as it is being *drawn in* by the high tensile elastic forces in the material. This *elastic rope* of converging fluid (to overstate the stress conditions within the converging material, for purposes of emphasis) being drawn in drags the surrounding annular fluid mass along with it, causing the pressure to rise to a somewhat greater value at section 2 than at section 1. This general ability to draw an elastic liquid forward by pulling on it is of course well known to those who process textile fibers, as well as to physiologists and veterinarians.

Similar to the derivation of Equation (2) a momentum balance between sections 2 and 3 may be shown to yield:

$$p_{A2} - p_3 = \rho V^2 \left(\frac{n}{2n+1}\right) + (P_{11} - P_{22})_2 - \left[\frac{2}{R^2}\int_0^R (p_3 + \tau_{11}) r dr\right]_3 + \frac{2L}{R}(\tau_{12})_w \qquad (7)$$

in which L denotes the axial distance between sections 2 and 3, and the subscript w denotes the wall stress at the fully developed flow conditions prevailing at section 3.

In the case of Newtonian fluids the first of the normal stress terms in Equation (7) is small and the second integrated stress under well developed flow conditions is identically zero. The excess pressure drop over the entry region, $p_{A2} - p_3 - (2L/R)(\tau_{12})_w$ is, however, not given correctly by $\rho V^2 (n/2n+1)$ because of our neglect of upstream pressure changes as well as the excess viscous drag in the inlet region of the small tube. The proper boundary layer analysis of flow in the small duct, for viscoelastic fluids, is a difficult one and the results are not central to the present analysis. Accordingly, we will simply replace the factor $(n/2n+1)$ with an adjustable parameter ϕ which, at intermediate Reynolds numbers, can be calculated from a boundary layer analysis and is given as 1.165 for Newtonian fluids by Collins and Schowalter (9). At Reynolds numbers greater than about 500 the occurrence of *vena contracta* effects appears to negate the boundary layer analyses so that in general the parameter ϕ must, at present, be evaluated experimentally (*11, 13, 20*), even in Newtonian fluids.

Under the conditions of primary interest in the present study, the first two terms on the right hand side of Equation (7) are generally appreciably larger than the third. In other words, momentum effects may be important and the normal stresses arising out of fluid stretching in the abrupt contraction at section 2 are large in comparison to the integrated normal stress term in the developed flow existing at section 3. Thus the third term on the right in Equation (7) is neglected and the last is combined with the pressure drop $p_{A2} - p_3$ to obtain:

$$\Delta p_c = \phi \rho V^2 + (P_{11} - P_{22})_2 \qquad (8)$$

in which Δp_c denotes the excess pressure drop beyond that due to a well developed pressure gradient, associated with flow in the entry region. This is the quantity usually reported in the literature as the *entry pressure drop*. It should be noted that though this term represents the change in the forces which would be read by conventional pressure gages mounted at sections 2 and 3, corrected for $(\tau_{12})_w 2\pi RL$, it does not represent the isotropic pressure difference between these sections in non-Newtonian fluids; for these materials the isotropic pressure is a function of deformation rate and varies radially across

the tube. This point is discussed in detail elsewhere [for example, by Savins (31)].

Equation (8) is one of the results sought. It is of interest in that it predicts, for sufficiently large normal stress differences $(P_{11} - P_{22})_2$ that the entry pressure drop will greatly exceed that in Newtonian fluids. That this occurs in practice is well known, dating from the pioneering study of Wood, Nissan, and Garner (36), and with data now available on systems ranging from elastic gels and molten polymers (3, 7, 24, 30) to solutions so dilute that the viscosity coefficient is constant and for which no direct measurement of elastic properties has been possible to date (2, 11), as well as for a wide variety of intermediate materials.

EVALUATION OF NORMAL STRESSES

The normal stress difference at the entrance plane of the tube, $(P_{11} - P_{22})_2$, may be calculated if the kinematics at this point and upstream from it are known, provided a proper constitutive approximation, applicable at the high deformation rates of interest, is available. The kinematics are indeed defined clearly by Equation (1*a*) and Figures 8 to 10. As a constitutive equation the convected Maxwell model which has previously been shown to be a useful approximation in many unsteady and rapid deformation processes (23) will be employed in a sample analysis. It is written:

$$\boldsymbol{\tau}' + \theta_{fl}\frac{\delta}{\delta t}\boldsymbol{\tau}' = 2\mu\mathbf{d} \tag{9}$$

$$\boldsymbol{\tau} = -p_o\,\mathbf{g} + \boldsymbol{\tau}' \tag{10}$$

Here, $\boldsymbol{\tau}$, $\mathbf{d}$, and $\boldsymbol{\tau}'$ denote the total stress, deformation rate and unnormalized stress deviator tensors; θ_{fl} and μ are the fluid relaxation time and viscosity while $\delta/\delta t$ denotes the contravariant convected derivative. The two physical property parameters, μ and θ_{fl} of Equation (9), do not portray the behavior of real materials at large deformation rates when they are assumed to be constants. In the case of the viscosity function the problem is normally met by simply permitting it to be a function of the invariants of the deformation rate tensor $\mathbf{d}$ and then, as a further approximation, considering the second invariant ($\frac{1}{2}$ *tr* $\mathbf{d}^2$) only (6). The same procedure will be applied here to both the viscosity and relaxation time functions, that is μ and θ_{fl} will be chosen as empirical functions of the second invariant of the deformation rate tensor. These functions will be evaluated from shearing and normal stress measurements in steady laminar shearing flows and applied to the elongational flow analysis of interest in this study, as an approximation.

Table 2. Relaxation Time Functions of Viscoelastic Fluids

Material	Γ, sec.$^{-1}$	θ_{fl}, millisec.	$\theta_{fl}\,\Gamma$
0.29% Carbopol 941	19	25	0.48
	40	12.5	0.50
	100	4.6	0.46
	200	2.1	0.42
	400	0.90	0.36
	500	0.70	0.35
0.20% ET-597 in water	1.31×10^3	6.81	8.9
	2.1	4.9	10.2
	3.7	3.4	12.5
	5.4	2.2	11.9
	7.5	1.8	13.5
	10.2	1.5	15.3
	11.7	1.4	16.4
	15.3	1.0	15.3
	17.2	0.95	16.3
5.0% polyisobutylene in decalin	13.6	33.8	0.46
	80.4	12.1	0.97
	5.4×10^2	4.07	2.2
	8.6×10^2	3.25	2.8
	1.6×10^3	2.30	3.7
	3.3×10^3	1.40	4.6
	5.4×10^3	0.96	5.2

Table 2 lists the relaxation times as well as the product of the relaxation time and deformation rate, for the fluids used by Marshal and Metzner (21). The relaxation time was evaluated from the measured stresses as (23)

$$\theta_{fl} = \frac{P_{11} - P_{22}}{2\,\tau_{12}\,\Gamma} \tag{11}$$

The normal and shearing stresses were obtained rheogonimetrically for the Carbopol solution and by means of capillary jet thrust measurements for the ET-597. The polyisobutylene data were obtained using both techniques. Table 2 shows that holding θ_{fl} constant, independent of the deformation rate, clearly represents an invalid approximation. A second equally simple, and more realistic approximation, is to hold the product of the relaxation time and deformation rate constant. This approximation is surprisingly good for the aqueous systems and will be employed for them. For the hydrocarbon system one may use:

$$\frac{1}{\theta_{fl}} = \theta_0 + \theta_1\,\Gamma \tag{12}$$

which is reasonable approximation at the higher deformation rates.

The kinematics of the flow process in the converging entrance region can be obtained through Equations (1*a*) and (1*b*). The deformation rate tensor in physical components is

$$d_{ij} = \begin{bmatrix} \dfrac{-2Q}{r^3} & 0 & 0 \\ 0 & \dfrac{Q}{r^3} & 0 \\ 0 & 0 & \dfrac{Q}{r^3} \end{bmatrix} \tag{13}$$

We will approximate the variation of the viscosity with deformation rate by use of a power law function of the second invariant of the deformation rate tensor (6):

$$\mu = K(II_{\mathrm{d}})^{(n-1)/2} \tag{14}$$

in which:

$$II_{\mathrm{d}} = (\tfrac{1}{2})\ tr\ \mathbf{d}^2 = \frac{3Q^2}{r^6} \tag{15}$$

and an appropriate deformation rate is $\sqrt{II_{\mathrm{d}}} = -\sqrt{3}Q/r^3$.

Combining Equations (1*a*), (1*b*), and (9) one obtains for the radial component of the normal stress deviator τ'_{11} in the flow direction:

$$\frac{d\,\tau'_{11}}{dr} + \left[\frac{r^3}{\theta_{fl}Q} + 4\right]\frac{\tau'_{11}}{r} = \frac{-4\mu}{\theta_{fl}r} \tag{16}$$

The term $r^3/\theta_{fl}Q$ is thus proportional to the reciprocal of the relaxation time-deformation rate product, and using the argument presented above, this group of terms will be taken as constant for the aqueous systems:

$$\frac{r^3}{\theta_{fl}Q} = \text{constant} = c_1 \tag{17}$$

Inserting Equations (17) and (14) into Equation (16) and solving the resultant first-order equation for the physical component of the normal stress one obtains:

$$\tau'_{11} = \frac{4c_1K}{A - 3n}\left[\frac{-Q}{r^3}\right]^n (3)^{(n-1)/2}\left[1 - \left(\frac{r_\infty}{r}\right)^{A-3n}\right] \tag{18}$$

n which $A = c_1 + 4$. The integration constant r_∞ in Equation (18) enters in order to satisfy the boundary condition that the stress goes to zero for a sufficiently large value of r, that is r_∞. This constant will remain undetermined throughout the analysis.

Solving similarly for the physical components of the other two normal stresses one obtains:

$$\tau'_{22} = \tau'_{33} = \frac{-2K(3)^{(n-1)/2}\, c_1}{c_1 - 3n - 2}\left[\frac{-Q}{r^3}\right]^n \tag{19}$$

Combining terms to obtain the normal stress difference appearing in the momentum balance, Equation (8) the result is:

$$(P_{11} - P_{22})_2 = (\tau'_{11} - \tau'_{22})_2$$

$$= (3)^{(n-1)/2} K c_1 \left(\frac{-Q}{r^3}\right)^n$$

$$\left[\frac{(6c_1 - 18n) + (12n + 8 - 4c_1)\left(\frac{r_\infty}{r_2}\right)^{c_1+4-3n}}{(c_1 + 4 - 3n)(c_1 - 3n - 2)}\right] \tag{20}$$

Noting that the product $K(-Q/r^3)^n$ is proportional to the shearing stress at the tube wall under conditions of well developed steady laminar flow, as prevails sufficiently far downstream from the converging region, Equation (19) may also be written:

$$(P_{11} - P_{22})_2 = \alpha_1 \tau_w \tag{21}$$

in which the term α_1 is a large and positive constant.

Combining Equations (20) and (8) one obtains a result which is readily verifiable experimentally:

$$\Delta p_c = \varphi\rho V^2 + \alpha_1 \tau_w \tag{22}$$

as it predicts a linear relation between the excess contraction pressure loss, Δp_c, and the shearing stress in the tube, provided the momentum term $\varphi\rho V^2$ is negligible.

Correspondingly for the hydrocarbon systems use of Equation (12) in place of Equation (17) may be shown to yield:

$$\Delta p_c = \varphi\rho V^2 + \alpha_1 \tau_w [1 + \alpha_2(\tau_w)^{1/n} + \alpha_3(\tau_w)^{2/n} + \ldots\ldots] \tag{23}$$

The extensive investigations of Bagley (3) into entry region pressure losses are in an ideal form for comparison with Equation (23) as the inertial term $\varphi\rho V^2$ is negligibly small in the case of molten polymers. Replotting the data presented in his Figure 1 gives $\Delta p_c/\tau_w$ as being nearly independent of τ_w at low values of τ_w and approaching a linear relationship at high values of τ_w. This is in qualitative agreement with Equation (23) though a stronger statement is not possible in view of the unknown values of the coefficients α_i for his fluids.

For dilute polymeric solutions unusually large entry region pressure losses are also wellknown; the data of Crawford discussed by Astarita and Metzner (2) yield values for the proportionality constant α_1 in Equation (21) as large as 500. Unfortunately most available end effect measurements for dilute solutions are at moderately high Reynolds number conditions, for which the inertial-viscous term $\varphi\rho V^2$ is neither negligibly small nor known. Thus, though the available data (2, 11, 13) may be shown to accommodate the linearity in τ_w predicted by Equation (21) they cannot be used to conform it with certainty, in the case of dilute solutions.

MEASUREMENT OF NORMAL STRESSES

Difficulties with all available techniques for measurement of normal stresses restrict these to polymeric solutions of moderate concentration. For example, in the cases of highly concentrated solutions or molten polymeric materials instabilities using the cone-and-plate geometry (10, 16, 19, 29, 35) restrict rheogoniometric measurements to uninterestingly low deformation rates (19, 35); the extent to which this may be resolved by using the theoretically superior parallel plate total force method does not appear to have been defined. Similarly the capillary jet technique (25, 28) is unwieldy with such materials, and the low Reynolds number of the flow introduces end-effect corrections which may be appreciable (25, 27). At the other extreme of very dilute solutions, both techniques are rigorously sound in principle but the low levels of the normal stresses developed frequently lead to overriding experimental errors. On the other hand the normal stresses developed in rapid elongational flows are much greater (1, 5, 21, 22), perhaps by as much as several orders of magnitude. Thus, Equation (21) suggests an experiment for measurement of normal stresses which is both sensitive and simple: namely the measurement of normal stresses through a measurement of the thrust of a jet of fluid issuing from an orifice placed on a large reservoir. If neither the normal stresses nor the momentum flux are assumed to vary with radial position across the jet a momentum balance on the jet yields:

$$T = [\rho V^2 - \tau_{11}]A_j \tag{24}$$

in which T is the measured thrust and A_j the cross-sectional area of the jet as it emerges from the orifice. Noting that the radial thrust τ_{22} is zero at the surface one may write:

$$\tau_{22} = 0 = -p + P_{22} \tag{25}$$

whence:

$$\tau_{11} = -p + P_{11} = P_{11} - P_{22} \tag{26}$$

Since $P_{11} - P_{22}$ does not vary with radial position this result, derived at the surface of the jet, must be true for all radial positions. Inserting this in Equation (24) gives:

$$P_{11} - P_{22} = \rho V^2 - T/A_j \tag{27}$$

It is seen that this technique directly leads to an explicit evaluation of the normal stresses; to be useful quantitatively these must, however, be relatable to the kinematics of the flow process. This requires the quantitative value of the parameter r_∞ of Equation (20); unless it is known measurements interpreted by means of Equation (25) would appear to be only of value for relative ordering purposes. The measurements may be expected to be very sensitive to fluid property variations, however, in view of the known large value of α_1 of Equation (22). The use of this experimental technique, or others equivalent to it, appears to have been suggested independently by at least two investigators (12, 26).

VARIATION OF ISOTROPIC PRESSURE IN CONVERGING VELOCITY FIELD

The isotropic pressure defined as the trace of the total stress tensor:

$$p = -\frac{1}{3}\tau_{ii} \tag{28}$$

may be calculated as a function of position in the converging velocity field from Equations (10), (18), and (19). At the entry plane of the small tube, the total outwardly directed stress, $-\tau_{22}$, is just equal to p_{A2}, as noted in Equations (3) and (4). Combining these equations one obtains:

$$(p)_2 = p_{A2} - (P_{11} - P_{22})_2 \tag{29}$$

$$= p_{A2} - \frac{\alpha_1 \tau_w}{3} \tag{30}$$

End effect measurements may be used to evaluate α_1 from Equation (22) and hence to obtain the isotropic

pressure at the inlet plane to the small duct as a decrement below p_{A2}, the gage pressure measured at this axial position. In the case of molten polymers the data of Bagley (3) and of Metzner, Carley, and Park (24) lead to $\alpha_1 \tau_w/3$ as great as 200 lb./sq. in., which is not, however, very large in view of the general pressure levels under which molten polymers are extruded. In the case of foamed polymer production operations in which a volatile component is present this may be of substantial importance, however.

For dilute polymeric solutions the differences between the isotropic and wall-tap pressures are more striking in view of the lower pressure levels of the entire flow process. Thus for the polyethylene oxide solution data cited by Astarita and Metzner (2) (WSR-301, at a concentration level of 250 ppm.), a maximum value for the $\alpha_1 \tau_w/3$ term in Equation (30) of 9.5 lb./sq. in. is obtained, at a flow rate giving a shear rate of 10^5 sec.$^{-1}$ in the small tube. If the entry is followed by a duct having a length to diameter ratio of 50:1, for example, the pressure decline in this duct is only 3.8 lb./sq. in. under the same conditions. Thus, were such a duct to discharge into the atmosphere the isotropic pressure at the duct entry would actually be (9.5 — 3.8) or 5.7 lb./sq. in. below atmospheric! Thus, the profile of the isotropic pressure vs. axial distance in the apparatus depicted in Figure 7 goes through a minimum at the entry plane to the small tube, and, depending on the overall dimensions of the system, this minimum value may be well below the ambient atmospheric pressure.

We are now in a position to give one interpretation of the haze in the central region of Figure 5. The fluid used was saturated with air at ambient conditions; the pressure p_{A2} was only about 1 lb./sq.in. above ambient. These facts imply that in the converging conical region degassing occurred at the isotropic pressure decreased. If this is the case one would expect not only the fluid upstream to be clear ($p \approx p_{A2}$) but to become clear again further downstream as $P_{11} - P_{22}$ again decreases to small values. This was indeed found to be the case. Thus, the available qualitative evidence supports the suggestion that the haze in Figure 5 corresponds to degassing in the region of low isotropic pressure.

CONCLUDING REMARKS

This paper was prepared to define the major macroscopic features of Lagrangian-accelerating velocity fields, as found at abrupt contractions, at high flow rates. The primary results to be noted are that normal stresses arising out of the fluid stretching or elongational deformations predominate in the central region of the flow, shearing deformations being totally absent, at a level of discrimination which would have detected consistent changes in velocity of less than 10% (Figures 8 to 10). The suggestion that the stresses generated due to elongational deformations overshadow the shearing stresses is emphasized by analyses of steady stretching used elsewhere to interpret the Uebler separational effect (22) and the abnormal resistances in flow through porous media (21); and through Equations (8) and (22) or (23) interprets the abnormal entry region pressure losses long known to occur in viscoelastic fluids.

Quantitative assessment of the predictions of the analysis, for the elongational flow described by the kinematics of Equation (13), are hindered by the form of the result [Equations (20) to (23)] which contains two parameters that are not known precisely in most cases. Comparisons made in the present work are checked semi-quantitatively, however, as they provide rational explanations for both the linearity of the excess entry region pressure drop noted by Bagley (3) in molten polymers and for the haze which develops near the entry plane in Figure 5, then disappears further downstream.

Of major importance is the observation that the kinematics of the converging velocity field are greatly simplified by the concomitant absence of shearing deformations at least at sufficiently high flows. This suggestion that shearing deformations are absent leads to an analytic simplification which is potentially of great importance in analysis of engineering flows of viscoelastic materials providing, hopefully, an alternate to boundary layer theory which tends to be inapplicable or of limited applicability, at the low Reynolds number–high Deborah number conditions frequently used during processing of these materials. Clearly the present analysis of the stress field, Equations (9) to (23), is more limited by the gross constitutive approximations made than by the complexities of the kinematics, and further analyses based on the well-defined kinematic conditions described by Equations (1*a*), (1*b*), and (13) appear warranted.

ACKNOWLEDGMENT

Dr. Hanswalter Giesekus supplied Figures 1 and 2; Professor J. H. Olson first advanced the degassing explanation of the haze present in Figure 5 and J. G. Savins provided the Carbopol data of Table 1. The Office of Naval Research, U.S. Navy, provided financial support for this study.

NOTATION

A = constant, equal to $c_1 + 4$
A_1 = cross-sectional area of upstream reservoir
A_2 = cross-sectional area of downstream tube
A_A = cross-sectional area of annular surface at Plane *2* of Figure 7
A_j = cross-sectional area of orifice
c_1 = equal to $r^3/\theta_{fl}Q$
$\mathbf{d}$ = deformation rate tensor
$f(\theta)$ = function of angular position, θ, defined in Equation (1)
$\mathbf{g}$ = metric tensor
K = coefficient in shear stress power law
L = tube length between control surfaces *2* and *3*
n = exponent in shear stress power law
N'_{Re} = generalized Reynolds number evaluated in downstream tube
p = isotropic pressure; p_o is the isotropic pressure in the assumed Maxwell constitutive model
p_1 = pressure in upstream reservoir
$(p)_2$ = isotropic pressure at control surface *2*
p_3 = radial stress (gage pressure) measured at wall at control surface *3*
p_{A2} = isotropic pressure at annular surface A_A
Δp_c = excess pressure drop over that due to a well-developed pressure gradient arising from flow into the entry region
P = deviatoric stress tensor
P_{11}, P_{22}, P_{33} = components of deviatoric stress tensor (physical components)
$(P_{11})_1, (P_{11})_2$, etc. = deviatoric stress component at control surfaces *1* and *2*, etc., respectively
q = actual volumetric flow rate
Q = volumetric flow rate function defined in Equation (1*a*)
r = radial coordinate in spherical coordinate system; r_2 is evaluated at control surface *2*
r^* = radial coordinate in cylindrical coordinate system
r_z = value of r at which the normal stresses become essentially zero
R = radius of downstream tube
T = thrust of fluid jet issuing from orifice
u = radial velocity component in upstream reservoir

u^* = local axial velocity within tube
V = average velocity in downstream tube
z^* = axial coordinate in cylindrical coordinate system

Greek Letters

α_1 = constant of proportionality, defined in Equation (21)
Γ = shear rate in steady laminar shearing flow
θ = tangential coordinate, Equation (1) only
θ_{fl} = relaxation time of fluid
μ = viscosity
ρ = density
Θ = half-angle of conical region, Figure 10
τ = total stress tensor
$\tau_{11}, \tau_{22}, \tau_{33}$ = normal stress components of τ
$(\tau_{11})_1, (\tau_{11})_3$, etc. = total stress components at control surfaces *1*, *3*, etc. respectively
τ_{12} = shear stress
$(\tau_{12})_w$ or τ_w = τ_{12} evaluated at the tube wall
τ' = stress deviator in Maxwell constitutive model
II_d = second invariant of the deformation rate tensor d
φ = adjustable parameter, to be determined experimentally

LITERATURE CITED

1. Astarita, G., *Ind. Eng. Chem. Fundamentals*, **6**, 257 (1967).
2. ———, and A. B. Metzner, *Atti Accad. Lincei*, **40**, VIII, 606 (1966).
3. Bagley, E. B., *Trans. Soc. Rheol.*, **5**, 355 (1961).
4. ———, A. M. Birks, and G. G. Warren, Film entitled "Polyethylene Flow Studies," Canadian Industries Ltd., McMasterville, Quebec (1961).
5. Ballman, R. L., *Rheologica Acta*, **4**, 137 (1965).
6. Bird, R. B., W. E. Stewart, and E. N. Lightfoot, "Transport Phenomena," John Wiley, New York (1960).
7. Boyce, R. J., W. H. Bauer, and E. A. Collins, *Trans. Soc. Rheol.*, **10**:2, 545 (1966).
8. Clegg, P. L., "The Rheology of Elastomers," p. 174, P. Mason and N. Wookey, eds., Pergamon Press, Nnew York (1958).
9. Collins, M., and W. R. Schowalter, *AIChE J.*, **9**, 804 (1963).
10. Cox, D., *Nature*, **193**, 670 (1962).
11. Drexler, L. H., M. Ch.E. thesis, Univ. Delaware, Newark, (1967).
12. Fabula, A. G., paper presented at fall meeting, Society of Rheology (1967).
13. Feig, J. E., M. Ch.E. thesis, Univ. Delaware, Newark, (1967).
14. Fields, T. R. and D. C. Bogue, *Trans. Soc. Rheology*, **12**, 39 (1968).
15. Hawkins, G. A., "Multilinear Analysis for Students in Engineering and Science," John Wiley, New York (1963).
16. Highgate, D., *Nature*, **211**, 1390 (1966).
17. Kaloni, P. N., *J. Phys. Soc., Japan*, **20**, 132 (1965).
18. *Ibid.*, **20**, 610 (1965).
19. King, R. G., *Rheol. Acta*, **5**, 35 (1966).
20. La Nieve, H. L., Ph.D. thesis, Univ. Tennessee, Knoxville (1966).
21. Marshall, R. J., and A. B. Metzner, *Ind. Eng. Chem. Fundamentals*, **6**, 393 (1967).
22. Metzner, A. B., *AIChE J.*, **13**, 316 (1967).
23. ———, J. L. White, and M. M. Denn, *Chem. Eng. Progr.*, **62**:12, 81 (1966).
24. ———, E. L. Carley, and I. K. Park, *Modern Plastics*, **37**, 133 (1960).
25. ———, W. T. Houghton, R. E. Hurd, and C. C. Wolfe., *Proc. Int. Symp. Second Order Effects Elasticity, Plasticity, Fluid Mech.*, 650 (1962).
26. Middleman, S., private correspondence (1967).
27. ———, and J. Gavis, *Phys. Fluids*, **4**, 963, 1450 (1961).
28. Oliver, D. R., *Can. J. Chem. Eng.*, **44**, 100 (1966).
29. Pearson, J. R. A., "Mechanical Principles of Polymer Melt Processing," Pergamon Press, New York (1966).
30. Philippoff, W., and F. H. Gaskins, *Trans. Soc. Rheol.*, **2**, 263 (1958).
31. Savins, J. G., *AIChE J.*, **11**, 673 (1965).
32. Schümmer, P., *Rheol. Acta*, **6**, 192 (1967).
33. Tordella, J. P., *Trans. Soc. Rheol.*, **1**, 203 (1957).
34. Uebler, E. A., Ph.D. thesis, Univ. Delaware, Newark (1966).
35. White, J. L., and A. B. Metzner, *Prog. Int. Research Thermophysical Transport Properties*, 748 (1962).
36. Wood, G. F., A. H. Nissan, and F. H. Garner, *J. Inst. Petrol.*, **33**, 71 (1947).

Manuscript received November 6, 1967; revision received May 13, 1968; paper accepted May 15, 1968.

Temperature Profiles of Molten Flowing Polymers in a Heat Exchanger

T. H. FORSYTH and N. F. MURPHY

Virginia Polytechnic Institute, Blacksburg, Virginia

The Graetz-Nusselt problem for polymeric flow in a constant wall temperature tube was studied, using a temperature-dependent power law rheological model and temperature dependent fluid properties. Theoretical results compare within 6% of experimental results. The fluid model predicts an experimentally observed temperature maxima at a reduced radius between 0.7 and 0.8 for cooling at low flow rates.

Heat transfer to flowing polymer melts and solutions is a very important, but complex, operation in polymer processing. Some of the factors which complicate the analysis of nonisothermal polymeric flow are:

1. The viscosity of nearly all polymers is non-Newtonian and temperature dependent.
2. Polymer melts and many polymer solutions exhibit viscoelastic behavior.
3. The density of polymer melts is temperature and pressure dependent.
4. Viscous heating effects and cooling by expansion can be significant.
5. Thermal properties are temperature dependent.

The system being considered is the classical Graetz-Nusselt problem for heat transfer to a fluid which is flowing in a circular tube. The fluid enters the tube at a constant temperature, T_1, and with a flat velocity profile. The tube has a constant wall temperature, T_w.

Many analyses of this problem have been reported (*1* to *4*), most of which are more applicable to polymer solutions than to polymer melts. Several solutions can, however, be applied to polymer melts. Topper (*5*) considered the heat generation term a constant across the tube radius

T. H. Forsyth is with the Dow Chemical Company, Midland, Michigan.